Influence of deformation temperature on texture evolution in HPT deformed NiAl

2014 IOP Conf. Ser.: Mater. Sci. Eng. 63 012154

(http://iopscience.iop.org/1757-899X/63/1/012154)

IOP Conf. Series: Materials Science and Engineering **63** (2014) 012154 doi:10.1088/1757-899X/63/1/012154

Influence of deformation temperature on texture evolution in HPT deformed NiAl

C Tränkner[1], R Chulist[1,2], W Skrotzki[1], B Beausir[3], T Lippmann[4], J Horky[5] and M Zehetbauer[5]

[1] Institut für Strukturphysik, Technische Universität Dresden, D-01062 Dresden, Germany
[2] Instytut Metalurgii i Inżynierii Materiałowej, Polskiej Akademii Nauk, PL-30-059 Kraków, Poland
[3] Laboratoire d'Etude des Microstructures et de Mécanique des Matériaux (LEM3), UMR 7239 CNRS and Université de Lorraine, Ile du Saulcy, F-57045 Metz Cedex, France
[4] Institut für Werkstoffforschung, Helmholtz-Zentrum Geesthacht, D-21502 Geesthacht, Germany
[5] Physik Nanostrukturierter Materialien, Fakultät für Physik, Universität Wien, A-1090 Wien, Austria
E-mail: christine.traenkner@tu-dresden.de

Abstract. NiAl is an intermetallic compound with a brittle-to-ductile transition temperature at about 300°C and ambient pressure. At standard conditions, it is very difficult to deform, but fracture stress and fracture strain are increased under high hydrostatic pressure. On account of this, deformation at low temperatures is only possible at high hydrostatic pressure, as for instance used in high pressure torsion. In order to study the influence of temperature on texture evolution, small discs of polycrystalline NiAl were deformed by high pressure torsion at temperatures ranging from room temperature to 500°C. At room temperature, a typical shear texture of body centred cubic metals is found, while at 500°C a strong oblique cube component dominates. These textures can be well simulated with the viscoplastic self-consistent polycrystal deformation model using the primary and secondary slip systems activated at low and high temperatures. The oblique cube component is a dynamic recrystallization component.

1. Introduction

NiAl is an intermetallic compound with B2 structure. Some of its characteristics make it a good candidate for technical applications at high temperatures, as for example the low density of 5.85 g/cm³ or the high melting point of 1638°C at stoichiometric composition as well as the very good oxidation resistance or the low coefficient of thermal expansion [1]. Nevertheless, NiAl is rarely used in industry because of its brittleness at low temperatures. The brittle-to-ductile transition temperature (BDTT) at ambient pressure is found at about 300°C. Below this temperature deformation is difficult as the critical resolved shear stress (CRSS) for activation of secondary slip along <111> or <110> is higher than the fracture stress. However, beside primary slip along <100> the activation of these slip modes is necessary in order to fulfill the von Mises criterion of five independent slip systems necessary for a homogeneous deformation of polycrystals. As shown in [2], at room temperature (RT) the fracture stress and fracture strain of NiAl is drastically increased by application of a high hydrostatic pressure. Thus, by shifting the BDTT below RT using high pressure torsion (HPT) [3], significant plastic deformation becomes possible at low temperatures.
It is the aim of the present work to investigate the texture evolution during HPT at lower temperatures than has been done before [4, 5]. Comparing the experimental textures with those derived from simulations of polycrystal deformation, conclusions about the slip systems activated at low temperatures can be drawn.

2. Experimental

The polycrystalline NiAl investigated has a nearly stoichiometric composition of (50.2 ± 0.1) at%Ni and (49.8 ± 0.1) at%Al. The initial microstructure and texture consist of an

average grain size of about 50 µm and a weak <111> fiber texture, respectively [4, 5]. Small discs of this material with a diameter of 8 mm and a height of 0.8 mm were deformed at room temperature and 500°C by HPT at a constant pressure of 8 GPa. According to [3], the shear strain in torsion is given by the relationship

$$\gamma = \frac{2\pi N r}{h}, \qquad (1)$$

with N = number of rotations, r = radius and h = height of the sample. For this work, two rotations are used resulting in a theoretical maximum shear strain of $\gamma \approx 60$ at the edge of the sample. The rotation rate was 0.2 rotations/min yielding a maximum shear strain rate of 0.1 s^{-1}.

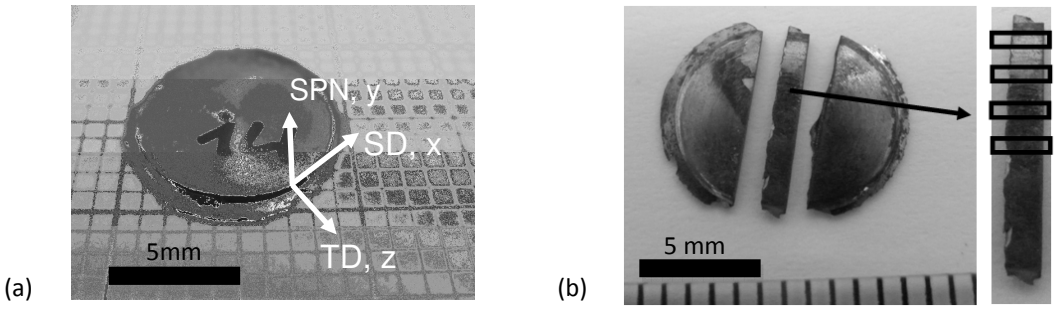

Fig. 1: Coordinate system of the deformed sample (a) and deformed and cut sample (b) with measurement positions on pin.

In Fig. 1a, the coordinate system is shown with SD being the shear direction, SPN the shear plane normal and TD the transverse direction pointing in radial direction. For texture measurements, small pins were cut by spark erosion along the radial direction of the deformed samples (Fig. 1b). The part of the samples investigated is a small volume near their edge.

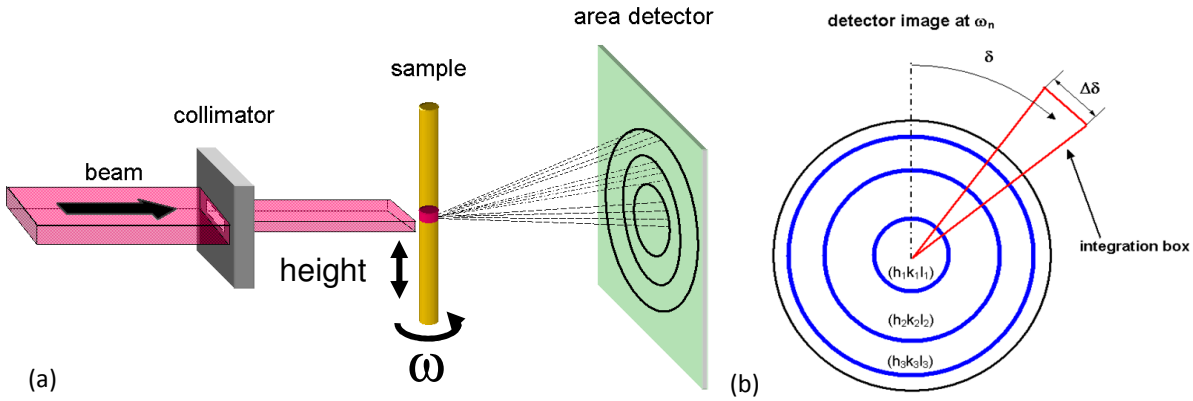

Fig. 2: Schematic diagram of experimental set-up for texture measurements with synchrotron radiation (a); read out of Debye-Scherrer rings by integrating the intensity along the rings in small steps (b), taken from [4].

Texture measurements were done by diffraction of synchrotron radiation at beamline HARWI II at DESY in Hamburg, Germany. In Fig. 2, the schematic set-up of the experiment is shown. Lattice planes fulfilling the Bragg equation reflect the beam. For each set of lattice planes, a Debye-Scherrer ring was then recorded with an area detector. For analyzing the texture, the first three rings corresponding to the {100}-, {110}- and {111}-lattice planes were used. The samples are rotated around the ω-axis by 180° in steps of 5°. To calculate the pole figures, the software StressTex [6] was used. The intensity of each pole figure is integrated in steps of $\Delta\delta=5°$ and the values of δ and ω are used to calculate the pole figures. Sections of the orientation distribution function (ODF) are then obtained by using the software LaboTex [7]. For more details on texture measurement with synchrotron radiation and data processing see [8].

Simulations have been carried out using the viscoplastic self-consistent (VPSC) model through the JTEX software. Initial texture measured from the undeformed sample was discretized into 10000 single orientations and used as input. The non-incremental tangent-based VPSC model was employed in its isotropic version concerning the interaction between the matrix and the grain [9]. More precisely, the finite-element-tuned model was used where the scaling parameter was 0.6 [10]. For low temperature torsion the {110}<100> and {112}<111> slip systems, for high temperature the {110}<100> and {110}<110> slip systems were used with equal critical resolved shear stresses. The strain-rate sensitivity index m used was 0.1 and work-hardening of the slip systems was not taken into account. The maximum shear strain of 2 was accomplished in steps of 0.02.

3. Results and discussion

The initial weak <111> fiber texture is shown in Fig. 3. During HPT it drastically changes with the changes strongly depending on deformation temperature. In this paper, the textures resulting from large strain shear deformation at room temperature and 500°C are compared.

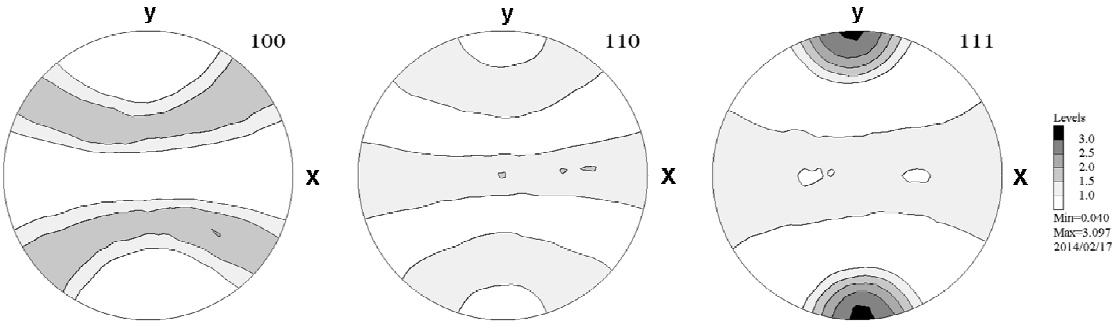

Fig. 3: Experimental pole figures of the initial <111> fiber texture.

In Fig. 4, the ODF sections for $\varphi_2=0°$ and $\varphi_2=45°$ are shown. The black circles denote the position of the ideal positions of simple shear texture components in bcc materials [11]. The black squares stand for the position of the cube component, which is a component not generated by shearing but by recrystallization. In Fig. 4a the ODF sections for the RT sample are shown. Here, the ideal simple shear texture components for bcc metals are found. The strongest texture component is the F component followed by D_1, J and $\bar{J}$, as also can be seen in Fig. 5a. Figures 4b and 5b show the ODF sections and the volume fractions of the texture

components of the sample deformed at 500°C. The texture is totally different compared to the RT sample. Only the F component of the ideal texture components can be found. Additionally, there is a very strong texture component which can be described as oblique cube component, as it is rotated around the transverse direction from the ideal position (see [5]).

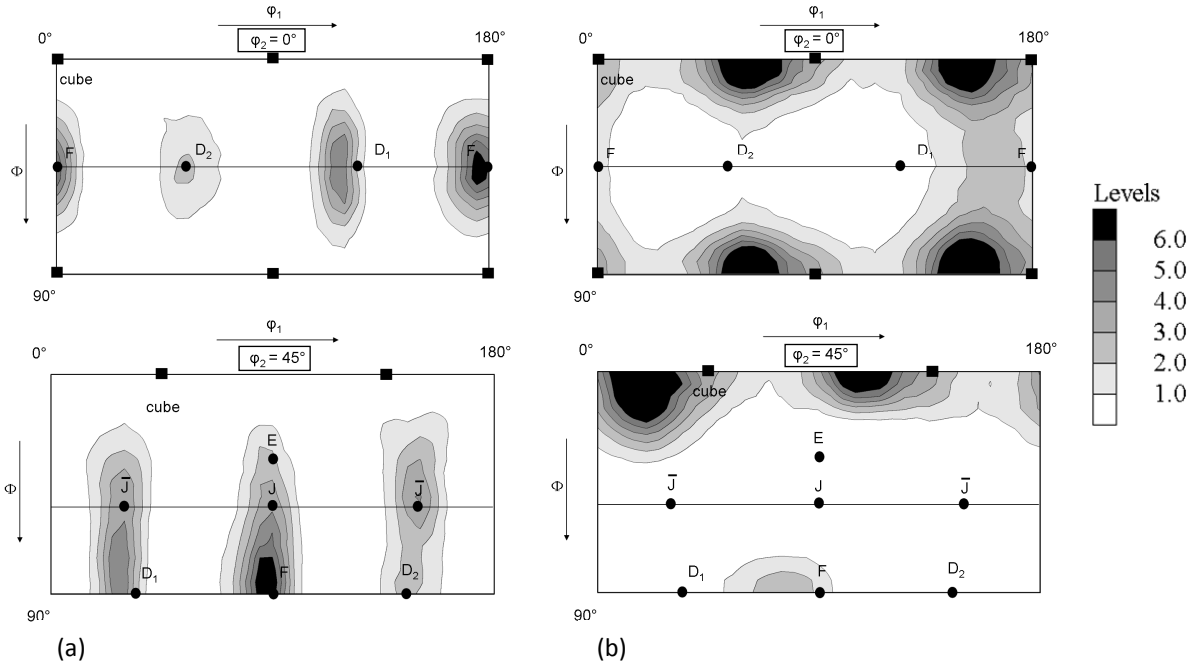

Fig. 4: Experimental ODF sections for φ_2=0° (above) and φ_2=45° (below) of the sample deformed at RT to a shear strain of γ = 58 (a) and at 500°C to a shear strain of γ = 50 (b).

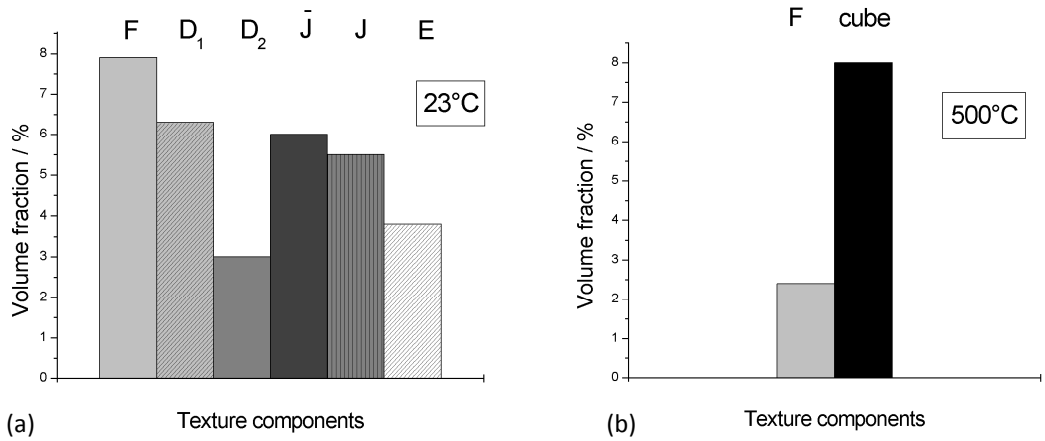

Fig. 5: Volume fraction of texture components found in the sample deformed at 23°C (a) and 500°C (b). The volume fraction of the other components is negligible. An orientation spread of ±10° was allowed around the maximum intensity of the components.

Changes in texture evolution with temperature can in part be explained with the change of secondary slip systems. At RT, the {110}<100> slip systems and – if pressure is sufficiently high – the {112}<111> slip systems can be activated. With increasing temperature, the CRSS of other secondary slip systems – those of {110}<110>slip – decreases. Therefore, at higher temperatures, 500°C, the primary slip systems {110}<100> and the secondary {110}<110> slip systems are activated. These two slip systems for an initial <111> fiber texture only lead to a strong F component, as simulations in [5] show. This is confirmed by simulations done with the software JTEX.

The results of the VPSC simulations done in this study are shown in Fig. 6. For HPT at RT the {110}<100> and {112}<111> slip systems were used with the same ratio of reference stresses. There is good agreement between simulation and experiment, compare Figs. 4 and 6. Using {110}<100> and {110}<110> slip systems, also with the same proportion, for high temperature deformation, nearly all texture components vanish except those of a strong F component and of very weak J and $\bar{J}$ components.

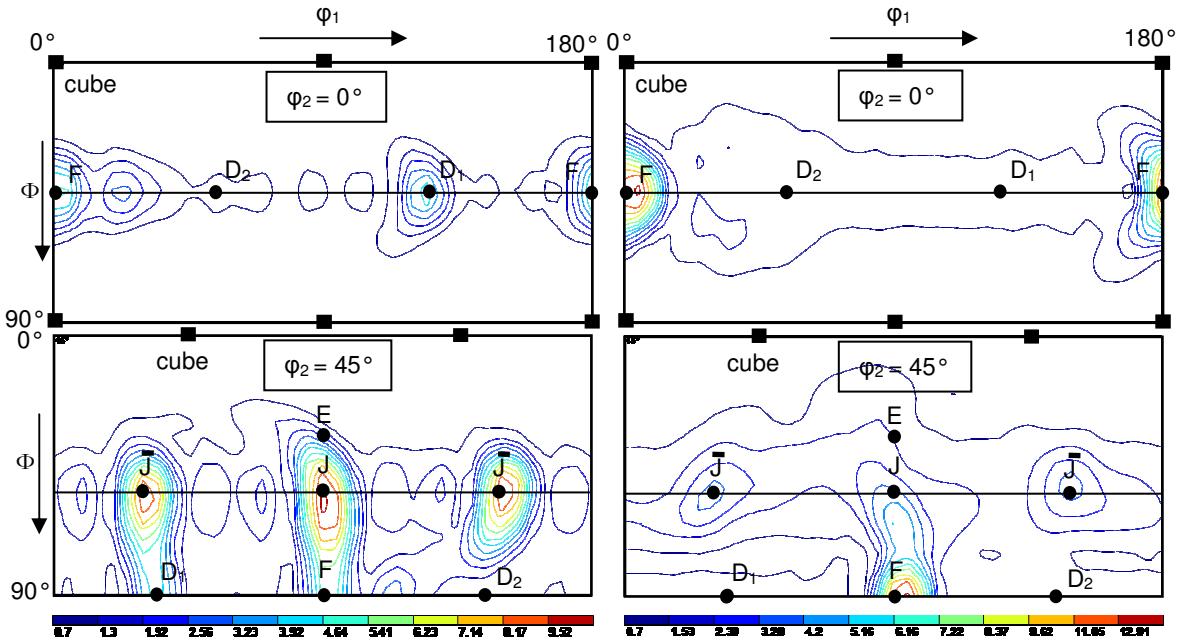

Fig. 6: Simulated ODF sections for φ_2=0° (above) and φ_2=45° (below) for low temperature (a) and high temperature shear (b).

The oblique cube component does not appear in the simulated textures as it is not generated by shear deformation but by dynamic recrystallization. Cube oriented nuclei during growth will be further deformed just rotating around the transverse direction, till - at a critical shear strain - another recrystallization event sets in. Thus, the recrystallization component appears in the ODF as an oblique cube component, see [5].

4. Conclusions

Texture evolution in HPT deformed NiAl strongly depends on deformation temperature. Room temperature deformation leads to the simple shear texture found in bcc metals. For deformation at 500°C a totally different texture is found with a strong oblique cube component and a weak F component.

The difference can be explained by the activation of different secondary slip systems, which causes the different intensities of the ideal shear components, and the onset of dynamic recrystallization during deformation which leads to the oblique cube component.

Simulations done with the viscoplastic self-consistent model agree well with experimental results.

Acknowledgment

The help of T. Reiter with sample cutting is gratefully acknowledged.

References

[1] Bürgel R, Maier HJ and Niendorf T 2011 (4th edition) *Handbuch Hochtemperatur-Werkstofftechnik* (Wiesbaden: Vieweg+Teubner) ch. 6 p 463
[2] Margevicius RW and Lewandowski JJ 1994 *Metall. Mater. Trans.* **A 25** pp 1457-1470
[3] Pippan R 2009 *High-pressure Torsion – Features and Applications*, ch. 9 p 217 in: eds. Zehetbauer MJ and Zhu YT 2009 *Bulk Nanostructured Materials* (Weinheim, Germany: Wiley VCH)
[4] Klöden B 2006 *PhD-Thesis* Institut für Strukturphysik, TU Dresden
[5] Klöden B, Oertel C-G, Skrotzki W and Rybacki E 2009 *J. Eng. Mater. Technol.* **131** 011102
[6] Randau C, Garbe U and Brokmeier H-G 2011 *J. Appl. Crystallogr.* **44** pp 641-646
[7] LaboTex Version 3.0.24
[8] Wcislak L, Klein H, Bunge HJ, Garbe U, Tschentscher T and Schneider JR 2002 *J. Appl. Crystallogr.* **35** pp 82-95
[9] Molinari A, Canova GR, Ahzi S 1987 *Acta Metall.* **35** pp 2983-2994.
[10] Molinari A, Toth LS 1994 *Acta Metall. Mater.* **42** pp 2453-2458.
[11] Li S, Beyerlein IJ and Bourke MAM 2005 *Mater. Sci. Eng.* A **394** p 75